Journal of Materials Chemistry A

Accepted Manuscript

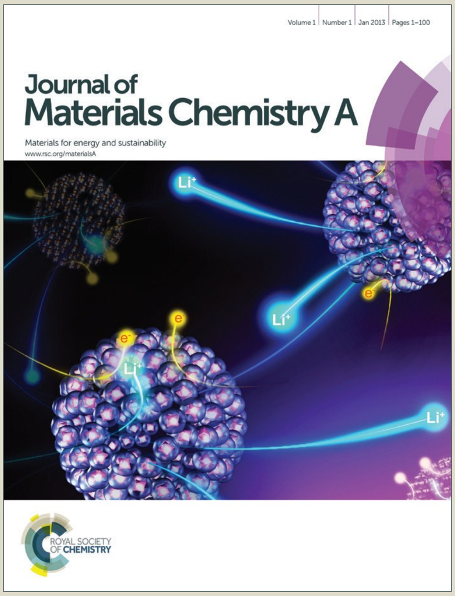

This is an *Accepted Manuscript*, which has been through the Royal Society of Chemistry peer review process and has been accepted for publication.

Accepted Manuscripts are published online shortly after acceptance, before technical editing, formatting and proof reading. Using this free service, authors can make their results available to the community, in citable form, before we publish the edited article. We will replace this *Accepted Manuscript* with the edited and formatted *Advance Article* as soon as it is available.

You can find more information about *Accepted Manuscripts* in the Information for Authors.

Please note that technical editing may introduce minor changes to the text and/or graphics, which may alter content. The journal's standard Terms & Conditions and the Ethical guidelines still apply. In no event shall the Royal Society of Chemistry be held responsible for any errors or omissions in this *Accepted Manuscript* or any consequences arising from the use of any information it contains.

ROYAL SOCIETY OF CHEMISTRY

www.rsc.org/materialsA

Fast and Reversible Photo-Responsive Wettability on TiO_2 based hybrid surfaces

Gwendoline Petroffe, Chao Wang, Xavier Sallenave,
Gjergji Sini, Fabrice Goubard, and Sébastien Péralta*

Laboratoire de Physicochimie des Polymères et des Interfaces (LPPI, EA 2528), Institut des Matériaux, Université de Cergy-Pontoise, 5 mail Gay-Lussac Neuville/Oise, 95000 Cergy-Pontoise Cedex, France
*E-mail : sebastien.peralta@u-cergy.fr

Abstract

A hybrid surface exhibiting fast and reversible switch between hydrophobicity and hydrophilicity states was prepared by spin-coating a porous TiO_2 layer by a mixture of TiO_2 nanoparticles with 11-(4-phenylazo)phenoxy)undecanoic acid (noted AzoC11 acid). The nanocomposite film corresponding to 10% AzoC11 acid/ TiO_2 mass fraction exhibited both very important and fast variation of contact angle (by more than 120°), along with an excellent reversibility. The wettability switching is explained by the *Trans*→*Cis*→*Trans* isomerization of the AzoC11 acid under light irradiation or heating. Upon *Trans*→*Cis* isomerization, optical absorption bands were found to exhibit drastic evolution, which origin is discussed in details by means of a time-dependent density functional theory study (TDDFT). Subsequent to these isomerization processes, various mechanisms explaining the wettability variations were investigated by comparing the results obtained by DFT calculations, wetting measurements for different surface ratios of AzoC11 acid under UV irradiation, and by analyzing the molecular structure and molecular surfaces of *Trans* and *Cis*-isomer of the AzoC11 acid.

Introduction

In recent years, superhydrophobic and superhydrophylic surfaces with water contact angle better than 150° and below 10°, respectively, meet a great scientific interest due to potential applications in self-cleaning[1], anti-fogging[2] or antireflective surfaces[3] and microfluid manipulations.[4,5,6] Furthermore, the rapid and reversible wetting transition between superhydrophilic and superhydrophobic states is one of the hot topics of research on developing functional materials in this last decade. Many investigations have show that

Journal of Materials Chemistry A Accepted Manuscript

besides the chemical nature of surfaces, the roughness and morphology also affect their wetting behaviour.[7,8]

The reversible wetting variation can be induced by the surface energy variations or/and the morphology modifications. In general, external stimuli, such as temperature[9,10], chemical treatment[11], electrical potential[12], pH[13,14,15,16,17] or light[18] can change the surface properties and the surface behavior. The use of materials with light-tunable wettability has promising applications because notably of avoiding the contact with materials which minimizes contaminations.

A wide number of inorganic materials are used for stimuli-responsive surfaces. Semiconductor oxides are well-known as stable, nontoxic and highly reactive materials which are able to induce a high wettability conversion between superhydrophobic and superhydrophilic state. In previous studies, surface wettability of light-responsive inorganic oxides under UV irradiation, such as ZnO[19], TiO_2[20,21,22] or V_2O_5[23] has been reported. However, the main problem with these materials is the too long time needed for the kinetic switching (several days for one cycle).[22,24]

As compared to inorganic materials, organic materials have many advantages in terms of the number of adaptable species, the potential for chemical modifications, and the reaction diversity. Such light-sensible materials are able to alter their properties reversibly, especially their wetting behaviour upon irradiation. These changes are often based on chromophoric groups of organic dyes such as azobenzene[4,25], spiropyran[7,26], coumarin[27] or cinnamate[28] which undergo a reversible izomerization under illumination. The wetting of azobenzene surfaces, for example, was tuned by alternation of UV and visible illumination during few minutes.[29] Unfortunately, the water contact angle variations (CAV) are very small (10° for smooth surface).[29,30] It is possible to increase the CAV using other solvents such as diiodomethane[31] or benzonitrile[32] instead of water.

Few authors have associated an organic layer with a semi-conductor oxide. Cho et *al.* have elaborated a roughness substrate based on layer-by-layer deposition of poly(allylamine hydrochloride) and SiO_2 nanoparticles.[33] This film was functionalized with photoswitchable azobenzene molecule the 7-[(trifluoromethoxyphenylazo)phenoxy]pentanoic acid (CF_3AZO). This system can be switched between superhydrophobicity and superhydrophilicity with 20 min UV irradiation and be reversible within 3 hours of visible light irradiation. Huang et *al.* have elaborated an original hybrid material based on filter paper in cellulose pre-coated by titanium ultrathin film.[34] With CF_3AZO monolayer self-assembled onto the titanium film, the water contact angle varied between 145,2° and 24,2° after 13 hours UV irradiation. The

Journal of Materials Chemistry A Accepted Manuscript

original high hydrophobicity was recovered after storage on the dark for one week. More recently, Wu *and al.* present a facile method of fabricating surface with reversibly tunable wettability. A mixing of poly(styrene-butylacrylate-acrylic acid) with TiO_2 nanoparticles in tetrahydrofuran (THF) was casting onto glass substrates.[14] The water contact angle of the film changed from the original 156° to about 0°, after irradiation with UV light for 2 hours. The initial state was recovered after heating of this superhydrophilic film at 150°C for 1 hour.

These three examples show the strong potential of hybrid materials to obtain significant variations in wetting. However, although the switching times are much faster compared to materials TiO_2, they are too slow to be considered for use in the field of microfluidics[35].

Aiming to prepare functional hybrid materials with both the advantages of inorganic nanoporous TiO_2 films and photosensitive moieties, We synthetized azobenzene functionalized titanium oxide derivatives with different degrees of coverage with azobenzene moieties. Preliminary, a organic photoswitchable molecule (Figure 1), the 11-(4-phenylazo)phenoxy)undecanoic acid (noted AzoC11 acid) was easily synthesized. Then, the photosensitivity of the AzoC11 acid in both solution and deposited on roughness controlled TiO_2 film was investigated. The azobenzene moieties of the AzoC11 acid/TiO_2 nanocomposite exhibited a reversible *Trans*→*Cis* isomerization transition upon irradiation with UV, leding to a change of the surface wettability. Thanks to the combination of this chromophore with a controlled roughness of TiO_2, faster reversible wettability switch is obtained as compared to the previous studies in this domain.[14,32,34]

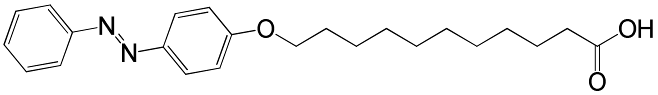

Figure 1: 11-(4-phenylazo)phenoxy)undecanoic acid (AzoC11 acid)

Experimental Section

Materials

4-phenylazophenol (98%), Triton X-100, acetyl acetone from Sigma-Aldrich, 11-bromoundecanoic acid (98%), potassium carbonate, titanium isopropoxide from Fisher Scientific, and Poly ethylene glycol from Merck were all used as received. Titanium

Journal of Materials Chemistry A Accepted Manuscript

nanoparticles (TiO_2 P25) was provided from Degussa. Tetrahydrofuran (THF) was dried by distillation from sodium metal/benzophenone and stored over 4-Å molecular sieves.

Water used for synthesis and contact angle measurements was purified by a Milli-Q system (resistance 18 MΩ).

Techniques of analysis

^1H and ^{13}C NMR spectra were recorded on a Bruker Avance DPX 250 MHz spectrometer. Chemical shifts are given in ppm using the residual solvent signal ($CDCl_3$) as an internal reference. Fourier transform infrared (FTIR) were recorded using a Bruker Tensor 27 spectrometer. The sample was pressed into KBr pellets. UV-visible measurements of the azobenzene derivative were performed at room temperature in spectrometric grade tetrahydrofuran solutions using a Jasco V570 spectrometer and an analysis cell with an optical path length of 10 mm.

Photoisomerizations *Trans* → *Cis* and *Cis* → *Trans* were realised from a UV lamp (15 W, λ_{max}=365 nm, Intensity at 2.0 cm = 1.5 mW/cm^2, Vilber Lourmat VL-215.LC) and blue light (150 W, λ_{max}=410 nm, Intensity at 2.0 cm = 21.5 mW/cm^2, Fort GLI 156), respectively. In all cases, the samples were placed at 2.0 cm.

The atomic force microscopy (AFM) experiments were performed in tapping mode with a Nanoscope V controler coupled at Icon microscope from Bruker. Measurements were carried out in air at room temperature. For each sample, AFM images were recorded on at least four samples and in several places in order to check the reproducibility of the displayed images.

Contact angles (CA) were determined using a DSA10-Mk2 (Krüss, Germany), out under air at room temperature, with 15 μL ultrapure water drop. The contact angles of the superhydrophilic surface are arbitrarily set at 10° because it is very difficult to obtain a reliable measurement of the superhydrophilic surface. For each samples, contact angles were measured on about three samples; fives drops per sample were analyzed. The reported contact angle values correspond to the average of all measurements with an error bar corresponding to the standard deviation.

The molecular areas are estimated by extrapolation of the surface pressure isotherm obtained on a Langmuir trough (model 611 from Nima). The spreading solution was AzoC11 acid dissolving in chloroform at concentration of 0.4 mg/ml. To obtain the molecular area of *Cis* form of AzoC11 acid, the spreading solution was previously irradiated with UV light for 10 min. The monolayer was compressed with a barrier speed of 20mm/min and the subphase was

Journal of Materials Chemistry A Accepted Manuscript

Journal of Materials Chemistry A Accepted Manuscript

the ultrapure water at 20±1°C. The molecular areas of AzoC11 acid correspond at the average of 5 extrapolations of surface pressure isotherm.

The layer thicknesses are the average of 10 measurements on two samples. The measurements are obtained by profilometry (Dektak 150 form Veeco).

Synthesis of 11-(4-phenylazo)phenoxy)undecanoic acid (AzoC11 acid):[36,37]

To a solution of 4-phenylazophenol (1.12 g, 5.6 mmol) and 11-bromoundecanoic acid (3 g, 11.2 mmol) in 150 mL of absolute ethanol was added dry potassium carbonate (1.58 g, 16.8 mmol). The mixture was stirred at reflux for 48h. After cooling, the ethanol was evaporated and the residu was dissolved in chloroform (200 mL). The organic layer was washed with HCl 2M solution (2×50 mL) then water (3×50 mL), dried over $MgSO_4$ and concentrated. The product was purified by recrystallization from acetonitrile to give an orange solid (1.15 g, 54%). ^{1}H NMR ($CDCl_3$) δ = 7.94 - 7.87 (m, 4H, *Ar*-N=), 7.54 - 7.43 (m, 3H, *Ar*), 7.01 (dd, *J* = 6.9 Hz et *J* = 2.1 Hz, 2H, *Ar*-O), 4.04 (t, *J* = 6.5 Hz, 2H, CH_2O), 2.30 (t, *J* = 7.3 Hz, 2H, CH_2CO), 1.85 - 1.76 (m, 2H, CH_2CH_2O), 1.67 - 1.61 (m, 2H, CH_2CH_2CO), 1.50 - 1.42 (m, 2H, $CH_2CH_2CH_2O$), 1.31 (m, 10H, CH_2). ^{13}C NMR ($CDCl_3$) δ = 179.2, 161.8, 152.6, 146.7, 130.3, 129.0, 124.9, 122.5, 114.7, 68.4, 34.4, 33.9, 29.4, 29.3, 29.2, 29.1, 29.0, 26.0, 24.6. IR (cm^{-1}): 2936, 2921, 2849, 1709, 1606, 1586, 1499, 1479, 1435, 1309, 1281, 1249, 1221, 1146, 1019, 845. Anal. Calcd for $C_{23}H_{30}N_2O_3$: C, 71.94; H, 7.90; N, 7.34. Found: C, 72.22; H, 7.91; N, 7.32.

Preparation of Substrates

The substrates are composed of a glass slide with a coating of a dense and nanoporous TiO_2 films.[38] All microscope slides from RS France were subsequently cleaned in a beaker of diluate Hellmanex solution (5%) at least 30 min at 50°C, rinsed with ultrapure water, sonicated for 10 min in ethanol, before being treated for 10 min by UV-ozone treatment (UVO cleaner 42 Jeligth). The glass substrates were used immediately.

A dense layer of TiO_2 is applied by spin coating from a precursor of TiO_2 solution. For preparation of the solution of the TiO_2 precursor, 7 drops of nitric acid (70%v/v) and 500 µL of water were added at 20 ml of pure ethanol. The solution was stirring during 30 min. 1.5 mL of titanium isopropoxide was added at this solution. The solution was mixed 24 hours without light. The TiO_2 solution was deposited by spin-coating on the microscope slides at 3000 tr/min during 60 sec. The layers are then annealed at 500°C for 15 min. The thickness measured by profilometer was about 80 nm.

A nanoporous layer of TiO_2 is applied by spin coating from a TiO_2 paste. For preparation of the TiO_2 paste, 100 mg of TiO_2 nanoparticles was dispersed in 10 mL of ultrapure water by sonicated for 10 min. 100 µL of acetyl acetone, 120 µL of acetic acid and 100 µL of Triton X-100 were added. The mixture was vigorous stirring for get a colloidal state. 120 mg of poly ethylene glycol (PEG, Mw = 4000 $g.mol^{-1}$) was employed as blowing agent. With magnetic bar stirring, this colloidal TiO_2 was equally mixed for 24 hours followed by spin coating deposition on the microscope slides coved with the dense TiO_2 layer at 2800 tr/min during 40 sec. Finally, the substrate was gradual annealed at 550°C, over 30 min. A 1000 nm thick film was obtained, as measured by profilometer. These titanium layers allow to induce a roughness at substrates and promote adhesion of the active layer during the spin coating.

Preparation of AzoC11 acid/TiO_2 nanocomposite films

The nanocomposite film is composed of mixture of the AzoC11 acid and TiO_2 nanoparticles (P25) in THF. 100 mg of TiO_2 nanoparticles were dispersed in 2 mL of THF by sonication for 10 min. 5, 8, 10, 15 or 25 mg of AzoC11 acid was added at this mixture. The solution was noted x% AzoC11 acid/TiO_2. After 24 hours of vigorous stirring, the mixture was a uniform milky liquid slighty orange. The AzoC11 acid/TiO_2 solutions were spin coated on the substrates at 2800 tr/min for 40 sec. Visually, the samples initially whitish become slightly orange. This nanocomposite film provides easily a structured surface.

Computational methodology

DFT[39] calculations employing the B3LYP[40,41] and ωB97XD[42] functionals were perfomed with Gaussian 09 program.[43] The geometry optimizations for all the molecules were carried out without symmetry constraints and were followed by frequency calculations. Given that several properties of this compound depend principally on the pi-conjugated backbone, a limited alkyl chain without the carboxylic group was considered for the calculation of the optical properties and for the solvation energy of the *Cis*-isomer. The spectroscopic properties of the molecules were calculated by mean of time dependent density functional theory method (TDDFT)[44,45,46,47,48] with the 6-31G(d) basis set. Up to 20 excited states were calculated and the theoretical absorption bands were obtained by considering a band half-width at half-maximum of 0.2 eV.[49] The interaction energies of the model water-complexes were calculated with respect to the isolated molecules at the ωB97XD/6-311+G(d) level in gas phase, and were corrected for the basis set superposition error (BSSE) by the counterpoise

Journal of Materials Chemistry A Accepted Manuscript

correction method of Boys and Bernardi.[50] The zero point energy (ZPE) corrections were also taken into account.

Results and discussion

Geometry and molecular orbitals (MO) of *Trans*- and *Cis*-isomers

The geometrical differences between the two isomers *Trans*- and *Cis*-AzoC11 acid are shown in Figure 2. While the *Trans*-isomer exhibits a perfectly planar π-system backbone, a C-N=N-C dihedral angle of -10.6° is found in the case of *Cis*-isomer, due to the steric hindrance between the phenyl rings.

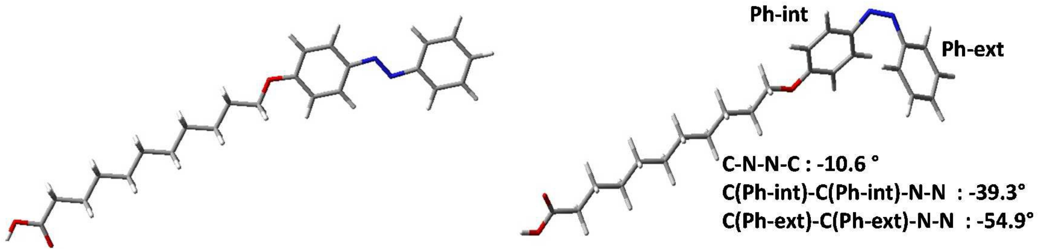

Figure 2: Geometries of *Trans*- and *Cis*-azoC11 acid as optimized at the B3LYP/6-31G* level by taking into account the solvent effect (THF). Some dihedral angles around the N=N bond in *Cis*-azoC11 acid are given.

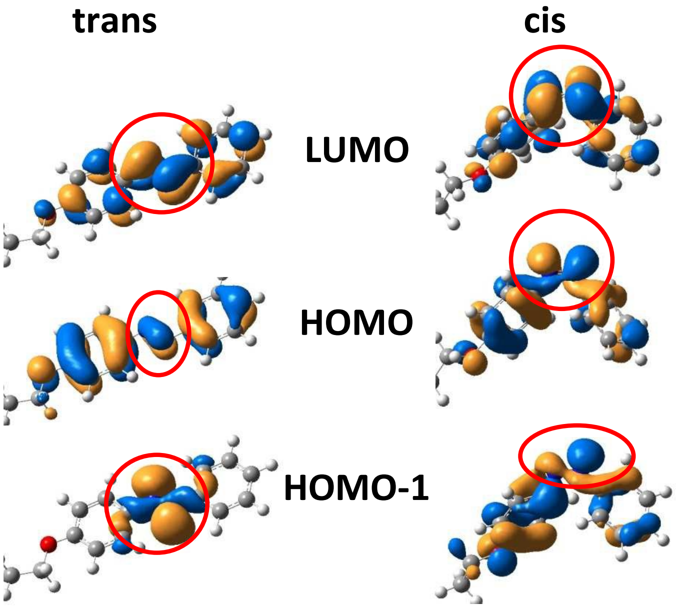

Figure 3: Selected set of MO plots corresponding to trans- and cis-azoC11 acid. The alkyl chains are hidden for sake of clarity. The encercled parts (red cercles) in each MO correspond to the contribution of the N-N fragment.

Journal of Materials Chemistry A Accepted Manuscript

Inspection of Figure 3 indicates two important differences between *Trans*- and *Cis* MOs: (i) increasing n-π mixture appears in the MO plots from HOMO-1 to HOMO in the case of *Cis*-isomer (ii) due to the non-zero C-N=N-C dihedral angle (-10.6°) in the *Cis* isomer, the π-conjugation efficiency decreases upon *Trans*→*Cis* isomerization. The energy order between the π-type (HOMO) and the n-type (HOMO-1) orbitals in the *Trans*-isomer is reversed in the case of *Cis*-isomer (dominant n-character in HOMO, dominant π-character in HOMO-1), which will be seen to impact the positioning and intensity of the absorption spectra. As for the LUMOs, they remain dominantly of N=N π–contribution for both isomers.

Absorption spectra of *Trans*- and *Cis* isomers in solution

The experimental UV-Vis spectra of AzoC11 acid in THF, before and after 40 sec UV irradiation, are given in Figure 4a, whereas the corresponding theoretical absorption spectra of *Trans*- and *Cis*-AzoC11 acid in THF are given in Figure 4b. Both *Trans*- and *Cis*-AzoC11 acid spectra present one low-energy band centered around 450 nm, and a higher-energy one peaking around 320 nm. Theoretical absorption spectra indicate that each band is due to a single excitation (Figure S1a of the ESI), principally of n→π* and π→π* character for the low- and high energy bands respectively (Figure 4b). In the case of the *Trans*-isomer, the theoretical n→π* transition (HOMO-1→LUMO) is symetry forbiden (zero oscillator strength, Figure 4b), due to the zero-overlap of the corresponding MOs (Figure 3). The non-zero experimental value for this band may be due to the geometrical deformations of the *Trans*-isomer in solution, which are absence in the theoretical results. Indeed, test calculations considering small deviations from the planarity around N=N bond (2°, 5°, 8°, and 10°) result in nonzero oscillator strength of 0.002, 0.003, 0.022, and 0.033 respectively for the n→π* transition (Figure S1b of the ESI).

Upon UV-irradiation of the *Trans*-isomer, the intensity of the π-π* transition band (~350 nm) decreases importantly and the maximum position is blue shifted to 315 nm. These important modifications are principally due to two effects: (i) becauce of the n-π nature mismatch between HOMO-1 and LUMO at the N=N moiety of *Cis*-isomer, the HOMO-1 – LUMO overlap (impacting the transition intensity) is reduced importantly, and (ii) in the case of the *Cis*-isomer, the π-π* excitation principally corresponds to HOMO-1→LUMO transition (77%), involving a larger gap as compared to HOMO-LUMO gap for the *Trans*-isomer, consequently resulting in the observed blueshift. Similar arguments apply to the n-π* transition band at 442 nm: due to the n-π mixing, the n-π* transition in the case of the *Cis*-isomer becomes less forbiden, resulting in the slight increase in the intensity of the low-

Journal of Materials Chemistry A Accepted Manuscript

Journal of Materials Chemistry A Accepted Manuscript

energy band. Upon *Trans* →*Cis* isomerisation of AzoC11 acid in THF solution, the absorption spectra thus exhibit important changes in the intensity and position of the bands. The UV-Vis spectroscopy presents consequently an easy method to follow the *Trans* → *Cis* isomerization.

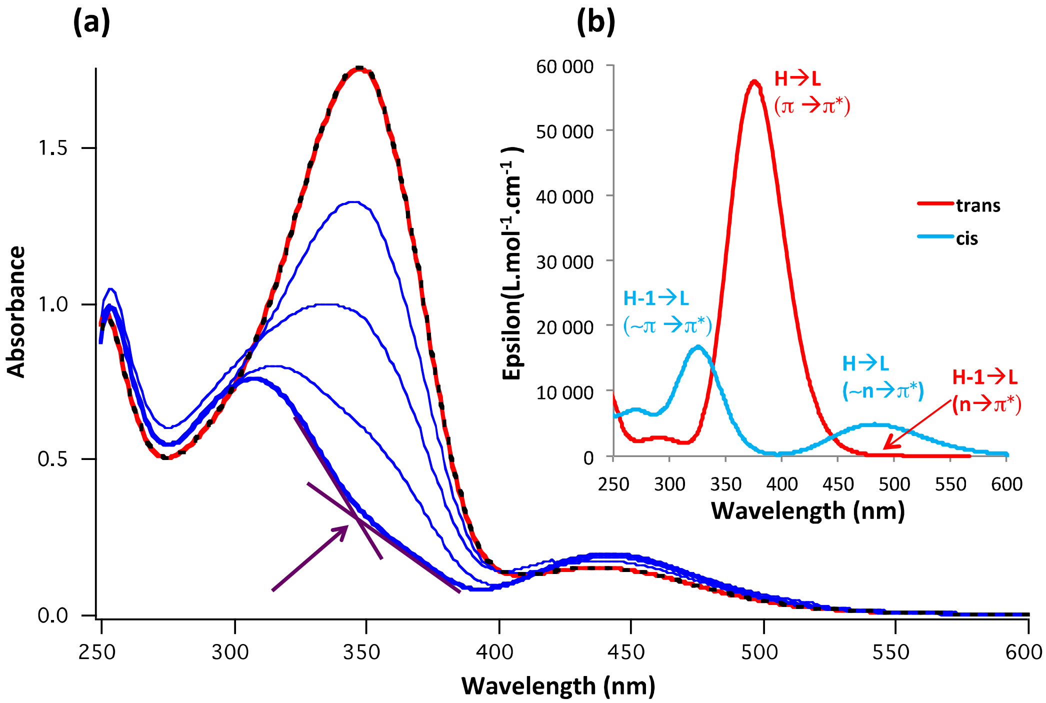

Figure 4: (a) UV-vis spectra of AzoC11 acid in THF solution (C=10^{-4}mol.L^{-1}) before (red curve), during (blue curve) and after (blue bold curve) UV irradiation and after the blue irradiation (black dotted curve). The highlighted discontinuity of the high-energy band of the *Cis*-isomer is supposed to be due to the presence of some *Trans*-isomer. Inset (b) theoretical absorption spectra obtainer at the TDB3LYP/6-31G* level. The dominant transitions are also indicated for each band.

The experimental UV-Vis spectra of AzoC11 acid in THF during UV irradiation (Figure 4a), suggests that some amount of the *Trans*-isomer is still present in solution. Indeed, after 40 sec of UV irradiation (blue bold curve), the high-energy band exhibits a discuntinuity of the right-hand part (highlighted by an arrow, Figure 4a), which position fits perfectly with the maximum position of the *Trans*-isomer. This conclusion is supported by the similar positions of the absorption onset (Figure S2 of the ESI) between the two bands in the experimental spectra, both features (discontinuity and identical onset) being absent in the theoretical absorption spectra (Figure 4b). A possible explanation for this mixture could be given in terms of relative stability of the *Trans*-and *Cis*-isomers, the later one being ~11 kcal.mol^{-1} higher in energy as compared to the *Trans*-isomer (ωB97XD/6-311+G** level in THF). Finally, after subsequent blue illumination, *Cis*→*Trans* isomerisation occurs with very high

Journal of Materials Chemistry A Accepted Manuscript

yield, as the spectrum of the *Trans*-azobenzene is totally restituted. The restituted spectrum (black dotted line) is superposed on the initial spectrum (red solid line) in Figure 4a.

Despite the presence of some mixture of *Cis*- and *Trans*-isomers in solution, the Figure 4a indicates that the intensity of the high-energy absorption band of the AzoC11 acid upon UV and Visible light irradiation exhibits important variations and is almost totally reversible. The Figure 5 shows the normalized absorption intensities of the the AzoC11-acid high-energy band for several UV↔Vis irradiation cycles.

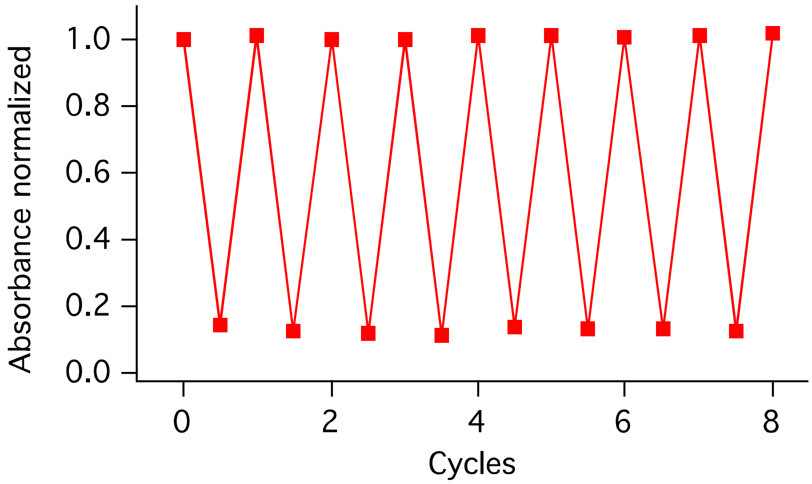

Figure 5: Reversible *Trans-Cis* izomerisation of the AzoC11 acid in THF (C=5x10^{-5}mol/L) under 2 min UV irradiation and 2 min blue light irradiation. The location of the markers indicate the normalized absorbance of the high-energy absorption band (at 348 nm) of the AzoC11 acid upon UV and Visible light irradiation.

The absorbance maxima- and minima at 348 nm correspond respectively to predominantly *Trans*- and *Cis*- AzoC11 acid. The *Trans*→*Cis* and *Cis*→*Trans* isomerization of a solution of AzoC11 acid is fast (less than 4 min for a full cycle) and completely reversible, making the AzoC11 acid a good candidate for developing photosensitive surfaces.

Morphology Characterization of nanocomposite films

The nanocomposite film is composed of mixture of the AzoC11 acid and TiO_2 nanoparticles (P25) in THF spin coated on the titanium substrate. Optimization of a large and reproducible photoresponsive switch is based on the control of wettability of the film, which is generally influenced by the morphology and surface free energy. The former is often exhibited as the surface roughness, and the latter is usually displayed as the change in dipole moment.

Firstly, the roughness of the film was estimated from AFM height images before and after the AzoC11 acid/TiO_2 deposition (Figure 6).

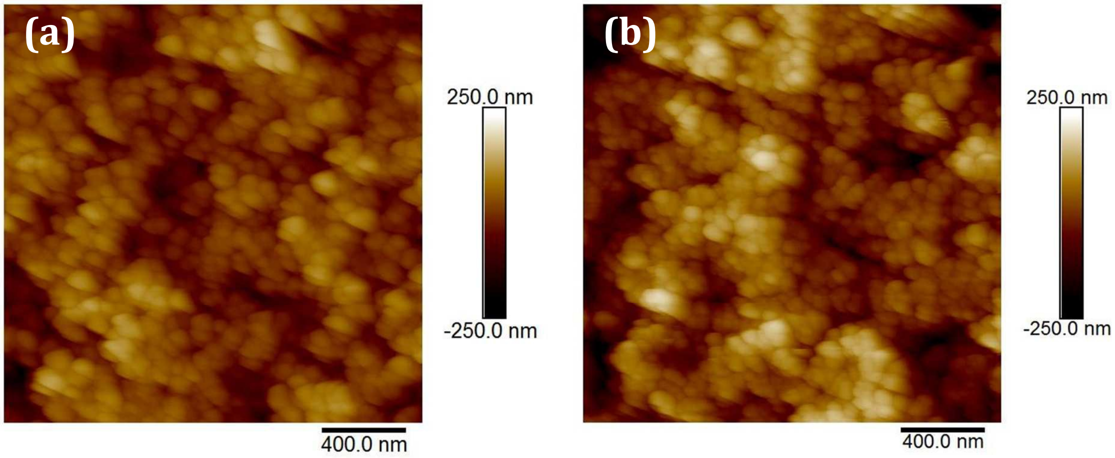

Figure 6: AFM images of the substrate: dense + nanoporous TiO_2 layers (a) and the mixture of 10% wt AzoC11 acid/TiO_2 on dense + nanoporous TiO_2 layers (b) (2 µm × 2 µm)

The AFM images of substrate reveal the nanoporous structure of the TiO_2 layer. The pores are formed by the calcination of the blowing agent (PEG, Mw = 4000 $g.mol^{-1}$). The average size of grains is 300 nm. These grains are therefore the result of the aggregation of nanoparticles whose initial diameter is 20 nm. The images of pure TiO_2 film and the AzoC11 acid/TiO_2 layer are very similar. However the slighty orange color of the sample shows that the organic layer is present. No additional aggregates were observed between the image 6(a) and the image 6(b), AzoC11 acid forms a homogeneous layer on the surface. The active layer thus preserves the nanoporous nature of the substrate. Furthermore, AzoC11 acid appears to form a homogeneous layer on the nanoparticles surface without filling the nanopores. Indeed, root-mean-square roughness (R_{rms}) calculated on 5 images of 4 μm^2 were very close, respectively 49±4 nm and 64±3 nm for pure TiO_2 and AzoC11 acid/TiO_2 layer on the substrate.

AzoC11-acid/TiO_2 nanocomposite films: effect of surface-coverage on the contact angles.

Surface coverage ratios. The wettabillity of the nanocomposite films on nanoporous TiO_2 layers is followed by measuring the contact angle. The influence of surface-coverage on the contact angles was studied by considering the AzoC11-acid/TiO_2 weight ratios of 0, 5, 8, 10, 15 and 25 %. In order to correlate these weight ratios with the individual surface ratios of *Trans*- and *Cis*-AzoC11 acid on the TiO_2 nanoparticles, the molecular areas of *Trans*- and *Cis*- AzoC11 acid were estimated by extrapolating surface pressure isotherms. The molecular areas of 0.27±0.02 nm^2 and 0.39±0.08 nm^2 for the *Trans*- and *Cis*-isomers respectively were found, results also supported by the theoretical estimations of 0.26 nm^2 and 0.41-0.42 nm^2

Journal of Materials Chemistry A Accepted Manuscript

(see ESI: annexe III). The value of the *Trans* AzoC11 acid is comforted by the molecular area of *Trans* 4-octyl-[phenylazo-phenoxy] pentanoic acid estimated by Zhang (0.28 nm^2).[51] Based on these molecular areas and the specific area of TiO_2 nanoparticles P25 (55 m^2/g), the surface ratio of the AzoC11 acid on the nanoparticles can be estimated (see ESI: annexe IV). Surface ratios for the different mass fraction of AzoC11 acid are presented in the Table 1.

Mass fraction of AzoC11 acid/TiO_2	5%	8%	10%	15%	25%
Surface ratios with *Trans* AzoC11 acid	39±3%	62±5%	77±6%	116±9	193±14%[52]
Surface ratios with *Cis* AzoC11 acid	56±12%	89±19%	111±23%	167±34%	279±57%

Table 1: Surface ratios (in %) calculated as function the mass fraction of AzoC11 Acid

Note that an AzoC11 acid/TiO_2 weight ratio of ~10% seems to correspond to roughly 111 % of TiO_2 surface coverage with *Cis*-AzoC11 acid, but only 77% with *Trans*-AzoC11 acid.

Effect of surface-coverage on the contact angles. In the following, unless otherwise specified, the surface coverage ratios considered during the discussions will correspond to the surface ratios of *Trans*-AzoC11 acid will be considered (Table 1). The contact angles, corresponding to nanocomposite films with different AzoC11 acid/TiO_2 surface ratios, were measured and shown in Figure 7a.

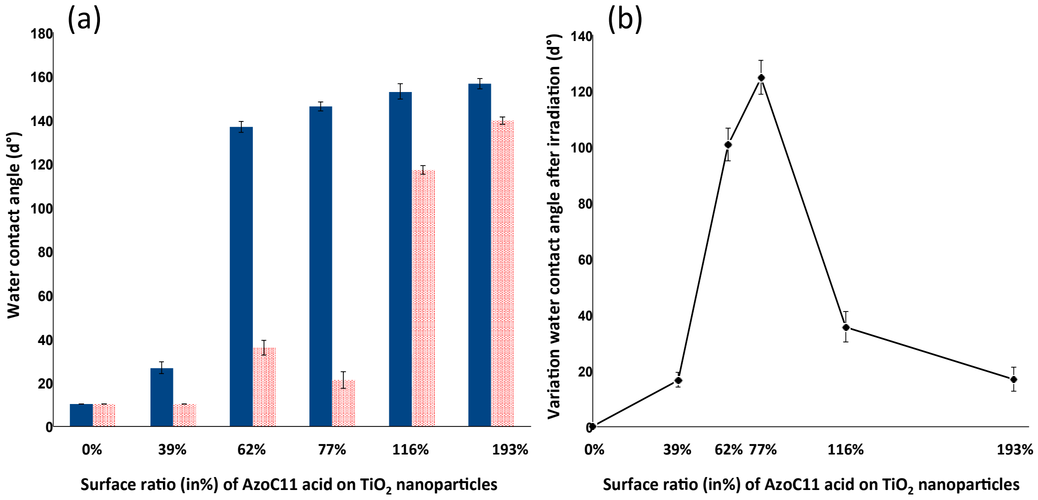

Figure 7 : (a) Initial water contact-angle for differences surface ratio of AzoC11 acid (full blue bars), and contact angle after 12 min of UV irradiation (patterned red bars).

(b) The variations of the contact angles between before- and after the UV irradiation are shown by the diamond markers (◆). The authors recall that the angles of superhydrophilic surfaces are arbitrarily set at 10°.

Journal of Materials Chemistry A Accepted Manuscript

Initial contact angles (ICA). In the absence of AzoC11 acid, the TiO_2 surface is superhydrophilic (the contact angle is less than 10°). Figure 7a suggest clearly that the increase of the ICA with increasing surface ratios between 0-193% is simply due to the increase in surface coverage with AzoC11 acid (Table 1). The ICA increase rapidly when the AzoC11/TiO_2 surface ratio of is smaller than 62%, but remain stable (close to 150 °) for larger surface coverage values. Modulating a surface state from a superhydrophilicity- to a superhydrophobicity state can thus be easily achieved by varying the amount of AzoC11 acid in the mixture.

Contact angles after UV irradiation. Contact angles after UV irradiation (CAAUV) are lower than the initial contact angles for all surface ratios[53], which could be explained by a competition between different processes: (i) *Trans*→*Cis* isomerization of the azobenzene function upon UV irradiation induces a variation in the dipole moment, which has been considered as the dominant factor influencing the surface energy upon isomerization.[54,55] Indeed, the theoretical dipole moments of the isolated *Trans*- and *Cis*-AzoC11 acid range respectively between 2.2-2.9 D and 3.6-6.1 D (B3LYP/6-31G** level "in THF"). While the absolute values of the dipole moments of AzoC11 acid on TiO_2 surface may be different as compared to the isolated molecules, their trend between *Trans*- and *Cis*- isomers is expected to remain identical. The polarity of AzoC11 acid thus increases after UV irradiation, in turn increasing the surface hydrophilicity and decreasing in contact angle. (ii) *Trans*→*Cis* isomerization additionally allows for the establishment of hydrogen bonds between the nitrogen lone pairs and water molecules, thus increasing the surface hydrophilicity. Indeed, HOMO plot of *Cis*-isomer (Figure 8a) shows both nitrogen lone pairs oriented outside with respect to the surface. Our test calculations on model *Cis*-AzoC11 acid----2H_2O complex clearly indicate establishment of efficient hydrogen bonds, with a net energy stabilization of 5.4 $kcal.mol^{-1}$, consistent with a typical value of ~3 $kcal.mol^{-1}$ per individual H-bond. On the contrary, the nitrogen lone pairs are little visible when the AzoC11 acid is in the *Trans* form, as also suggested by the shape of HOMO-1 (Figure 3). (iii). Upon UV irradiation, photogenerated holes diffuse to the TiO_2 surface and react with lattice oxygen of TiO_2 itself, resulting in the creation of oxygen vacancies at the surface.[56] These oxygen vacancies are presumably favorable for water adsorption.[57] Water molecules are both adsorbed on defect sites and dissociated, resulting in, generation of two hydroxyl groups on each defect [20,34,58] (Figure 8b). Increased hydrophilicity character of TiO_2 (and global) surface will consequently occur.

Journal of Materials Chemistry A Accepted Manuscript

The change in the contact angles after UV irradiation can thus result from a competition between these three factors. However, hydrophobicity-to-hydrophilicity switching times are much larger for the pristine titania surface as compared to TiO_2 surface covered with AzoC11 acid, suggesting that the third factor should be of minor influence in the above competition. This conclusion is also supported by the observation that decreasing the free surface of TiO_2 by increasing the surface coverage with AzoC11 acid, results in increased contact angle variation (Figure 8b).

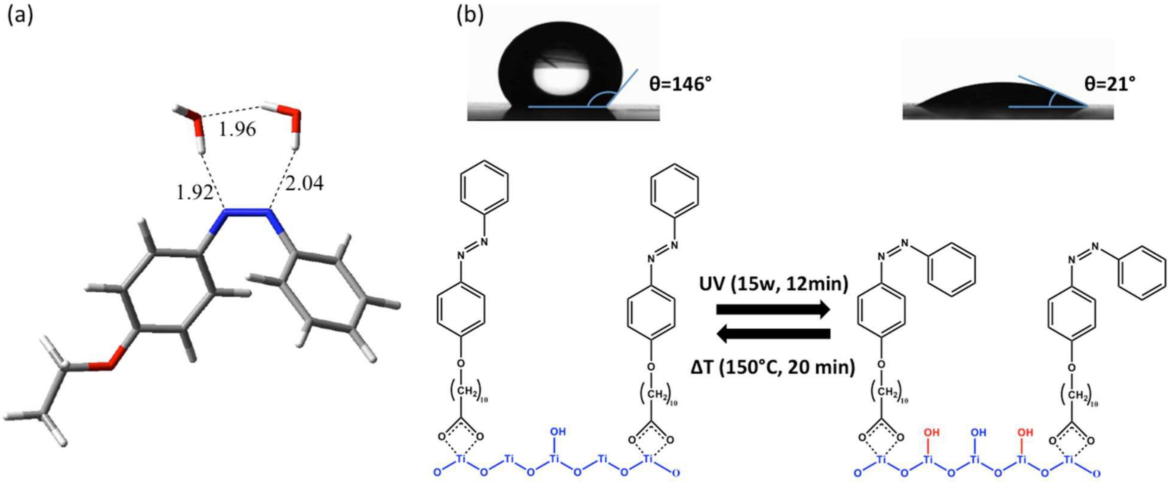

Figure 8: (a) Model *Cis*-AzoC11 acid----$2H_2O$ complex as calculated at the wB97XD/6-311+G(d,p) level by taking into account the effect of the solvent (water). The indicated distances are in Å.
(b) The different effects of UV irradiation on AzoC11 acid/TiO_2: azobenzene isomerization and hydroxyl photo-generation (in red)

Concerning the evolution of the CAAUV with the increasing surface ratio (Figure 7b), the smallest CAAUV corresponds to the pristine TiO_2 surface (0% surface ratio, Figure 8a). The increase in CAAUV in the presence of AzoC11 acid can be due to the fact that the *Trans*→*Cis* isomerization is not complete even after 40 min of UV irradiation (Figure 4). The CAAUV remain however less than 40° for surface ratios from zero to 77%, which is consistent with both the 77% of surface coverage ratio for the *Trans*-isomer and the 111% of surface coverage ratio for the *Cis*-isomer. Indeed, due to important geometrical modifications during *Trans*→*Cis* isomerization (increase in the molecular areas from 0.27 nm^2 to 0.39 nm^2), free room is needed around the *Trans*-azobenzene moieties.[59] The 77% surface ratio for the *Trans*-isomer (10% of weight ratio) thus corresponds to enough free room around *Trans*-azobenzene groups for the *Trans*→*Cis* isomerization to be sterically unhindered. As expected, the CAAUV rises dramatically when the surface ratio for *Trans*-isomer is greater at 100%, suggesting small degree of *Trans*→*Cis* isomerisation. This last effect is consistent with the

Journal of Materials Chemistry A Accepted Manuscript

insufficient free space around *Trans*-azebenzene groups for a sterically unhindered *Trans*→*Cis* isomerization.

Contact angle variations. The contact angle variations (calculated as ICA-CAAUV, Figure 7b) depend consequently on the composition of the AzoC11 acid/TiO_2 mixture. In line with the evolution of ICA and CAAUV, the contact angle variations initially increase due to the sharp increase in ICA whereas CAAUV remains small due to efficient *Trans*→*Cis* isomerization. The contact angle variation (ICA-CAAUV) reaches the maximum value of 124,5° when the AzoC11 acid/TiO2 mass ratio reaches 10%, which corresponds to the ideal value of roughly 100% for the surface ratio (coverage) with *Cis*-isomer. For surface ratios larger than this ideal value, the *Trans*-AzoC11 acid layer becomes very compact and the ICA continuous to remain large, but the azobenzene groups are less and less able to undergo *Trans*→*Cis* isomerization because of the increased steric hindrance, thus resulting in much larger CAAUV and smaller contact angle variation.

These results show that there is a good correlation between the variations of contact angle and the AzoC11 acid/TiO_2 surface ratios. The mixture at 10 % wt of AzoC11 acid, resulting in *Trans*- and *Cis*-surface ratios of roughly 77% and 111% respectively, is a good compromise between the amount of AzoC11 acid present at the surface of TiO_2 and ability to isomerize. In addition, for this fraction, the contact angle variation is very important and fast: over 124° after 12 min under UV irradiation.

Reversibility study

Figure 9 shows the evolution of water contact angles of the 10% wt AzoC11 acid/TiO_2 film as a function of the irradiation time under UV light (15W, λ_{max}=365nm) and heating at 150°C to induce a return to hydrophobic state.[60]

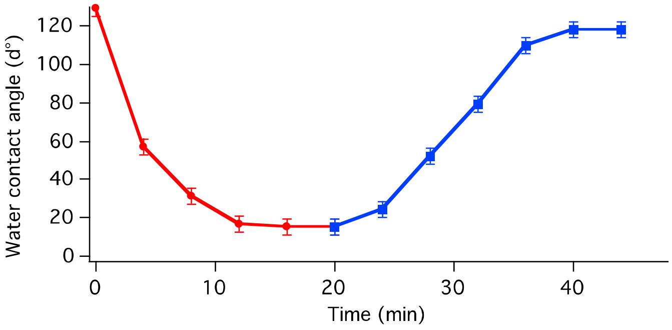

Figure 9: Water contact angle of the 10% wt AzoC11 acid/TiO_2 film as a function of the time of the UV irradiation (● in red)

and the time of heating at 150°C (■ in blue)

Upon UV irradiation, the azobenzene-groups in the film isomerize from the *Trans*- to the *Cis*-conformation, resulting in contact-angle decrease and film switching from superhydrophobic- to superhydrophilic state. Subsequent heating of AzoC11 TiO_2 films induces the reverse *Cis*→*Trans* isomerization, and the film hydrophobicity is accordingly recovered. The minimum of contact angle is obtained after 12 min of UV irradiation. After 20 min at 150°C, the contact angle recovers almost its initial value. The variation state is reversible and the full cycle is only 32 min. This is to our knowledge, both the most rapid kinetic encountered in the literature and with large variation as well.

The reversibility of the photoresponsive switch was estimated by following the evolution of the water contact angle of the 10% wt AzoC11 acid/TiO_2 film during several cycles (Figure 10). Each cycle corresponds to 12 min of UV irradiation followed by 20 min of heating at 150°C.

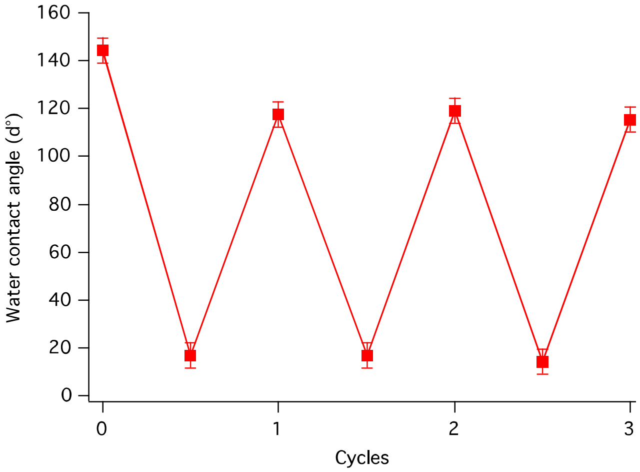

Figure 10: Reversible wettability transition of the 10% wt AzoC11 acid/TiO_2 film after several cycles of 12 min UV irradiation followed by 20 min at 150°C.

The water contact angle of the 10% wt AzoC11 acid/TiO_2 film decreased from 144° to 16° after 12 min UV irradiation. The quasi original high hydrophobicity was recovered after heating the sample at 150°C for 20 min. The process of reversible switching of the surface wettability was carried out over 3 cycles of UV irradiation and heating which indicates that the film has reproducible reversible wettability. While the contact angle after the first cycle is less than the initial contact angle (118° and 144° respectively), it remains however constant for the next cycles.

Journal of Materials Chemistry A Accepted Manuscript

Journal of Materials Chemistry A Accepted Manuscript

Different hypothesis can be emitted to explain the difference between the initial contact angle and the contact angle after the first cycle. The first hypothesis is based on the partial reversibility of the isomerization *Cis*→*Trans*. Unlike in solution, the mobility of AzoC11 acids is limited. When AzoC11 acids are in the *Cis* form, the molecules may be very close against each other. Some intermolecular interactions can thus be formed[61,62] and can limit the *Cis*→*Trans* isomerization of AzoC11 acid. To check this hypothesis, isomerizations *Trans*→*Cis* and *Cis*→*Trans* of 10% wt AzoC11 acid/TiO_2 film were followed by UV-Vis spectroscopy in reflectance mode. The absorbances values at 438 nm (in order to avoid the TiO_2 absorption at 348 nm) of 10% wt AzoC11 acid/TiO_2 film are reported in the Table 2 after each step.

	Initial	After 12min under UV Irradiation	After 20min at 150°C
Absorbance at 438nm	0.074	0.138	0.073

Table 2: Evolution of absorbance at 438nm of the 10% wt AzoC11 acid/TiO_2 film after one cycle of 12 min UV irradiation followed by 20 min at 150°C.

The absorption at 438 nm is characteristic of the n-π* transition. Under UV irradiation, the absorbance at 438 nm increases, asAzoC11 acid isomerizes from the *Trans* state to the *Cis* state. Also after the heating step, the absorbance at 438nm decreases, AzoC11 acid returns to the *Trans* state. Finally, the absorbance value after the first cycle (0.073) is very close to its initial value (0.074). It seems that the reversibility of the isomerization process in film is satisfying, thus suggesting that the decrease of the contact angle after the first cycle (from 144° to 118°) could not stem from uncompleted *Cis*→*Trans* isomerisation.

A second hypothesis is based on the process related to the substrate nature. Decrease in the contact angle after the first cycle have been already observed in the case of substrates based on TiO_2.[14,34,63] Whereas contact angles appear to be stable over the cycles in the case of is silica-based substrates.[64,65,66] In the previous section we showed that the photo-generated hydroxyl groups was not the dominant process in transitions between hydrophobic and hydrophilic states. However, this process may explain the differences of the initial contact angle and the contact angle after the first cycle. Indeed, while the isomerization process is fast (few minutes, Figure 9) relative to the desorption of hydroxyl groups photo-generated by UV, the return to the initial density of hydroxyl groups was shown to be very slow (several days).[22,30,67] Consequently, we suggest that the step at 150 °C during 20 min is not sufficient

Journal of Materials Chemistry A Accepted Manuscript

to allow a return to the initial density of hydroxyl groups. The variation of contact angle before and after UV irradiation, reported in the literature, on the TiO_2 pristine are superiors at 100°.[22,67] This assumption is supported by the estimation of the contact angle variations for a chemically heterogeneous surface by using the Cassie-Baxter law.[68] In the case of 10% wt AzoC11 acid/TiO_2 film, uncovered TiO_2 surface represents roughly 23% of the total surface, the rest of the surface being covered with *Trans*-AzoC11 acid. In this case, the contact angle variation estimated by means of the Cassie-Baxter law[69], is roughly thirty degree, which is consistent with the experimental difference of 26° between the initial contact angle and contact angle after the first cycle.

We finish this discussion by highlighting the dominant role of the isomerization process in wetting variations of on these hybrid materials as compared to the photo-generation of hydroxyl groups. However, the slow kinetic of desorption of these hydroxyl groups could explain the decrease in contact angle after a first cycle.

Conclusion

In this contribution, optimized wettability properties of a hybrid surface based on a mixture of TiO_2 nanoparticles with AzoC11 acid are presented. The method used in our study allows for an easy control of the covered surface ratio of AzoC11 acid on the TiO_2 nanoparticles. The maximum contact angle variations were found for a covered surface ratio of 77%.

Different processes were found to be responsible for the important changes in contact angle. In our system, contact angle variation induced by UV irradiation can be explained by the competition between two mechanisms, the hydroxyl groups photo-generation on the TiO_2 surface, and the isomerization of the azobenzene functions. This latter mechanism is preponderant, and has been demonstrated by molecular modelling to be due to two effects: (i) upon *Trans*→*Cis* isomerization, the dipole moment increases importantly, in turn resulting in hydrophilicity increase. (ii) the potential for the solvent (water) molecules to establish hydrogen bonds with the lone pairs increases in the case of *Cis*-isomer, again suggesting hydrophilicity increase by means of this effect.

Our hybrid surface combines the switching rapidity induced by organic surfaces and the large wetting variation observed on inorganic systems. The surface morphology exalts the wettability variation due to the presence of nanoparticles.

The main conclusion of this study is that the contact angle variations are important, reversible, and fast. The duration of a complete cycle is only 32 min. This is to our knowledge the shortest time found in literature (Table S1 of the ESI). While the kinetics of *Cis*→*Trans* isomerization is not yet fast enough to allow the integration of these materials in microfluidics devices, this study suggests these materials as good candidates for instance for self-cleaning or anti-fogging surfaces.

Journal of Materials Chemistry A Accepted Manuscript

Electronic Supplementary Information (ESI)

Theoretical absorption spectra of *Trans*- and *Cis*-AzoC11 acid in THF, Absorption onset on the UV-Vis spectra of AzoC11 acid solution, Theoretical estimation of molecular-areas, Expression of surface ratio, Values of wetting study, Comparison of contact angle variations versus the irradiation conditions.

Journal of Materials Chemistry A Accepted Manuscript

Notes and References

1. R. Fürstner, W. Barthlott, C. Neinhuis, and P. Walzel, *Langmuir*, 2005, **21**, 956–961.

2. L. Introzzi, J. M. Fuentes-Alventosa, C. a Cozzolino, S. Trabattoni, S. Tavazzi, C. L. Bianchi, A. Schiraldi, L. Piergiovanni, and S. Farris, *Appl. Mater. Interfaces*, 2012, **4**, 3692–3700.

3. X. Li and J. He, *Appl. Mater. Interfaces*, 2013, **5**, 5282–5290.

4. K. Ichimura, *Science*, 2000, **288**, 1624–1626.

5. A. Kausar, H. Nagano, T. Ogata, T. Nonaka, and S. Kurihara, *Angew. Chemie*, 2009, **48**, 2144–2147.

6. D. Baigl, *Lab Chip*, 2012, **12**, 3637–3653.

7. R. Rosario, D. Gust, A. a. Garcia, M. Hayes, J. L. Taraci, T. Clement, J. W. Dailey, and S. T. Picraux, *J. Phys. Chem. B*, 2004, **108**, 12640–12642.

8. D. Quéré, *Annu. Rev. Mater. Res.*, 2008, **38**, 71–99.

9. T. Sun, G. Wang, L. Feng, B. Liu, Y. Ma, L. Jiang, and D. Zhu, *Angew. Chemie*, 2004, **43**, 357–360.

10. W. Yuan, G. Jiang, J. Wang, G. Wang, Y. Song, and L. Jiang, *Macromolecules*, 2006, **39**, 1300–1303.

11. Z. Wang, L. Zhu, W. Li, and H. Liu, *Appl. Mater. Interfaces*, 2013, **5**, 4808–4814.

12. S.-S. Yoon and D.-Y. Khang, *J. Mater. Chem.*, 2012, **22**, 10625–10630.

13. G. B. Demirel, N. Dilsiz, M. Çakmak, and T. Çaykara, *J. Mater. Chem.*, 2011, **21**, 3189–3196.

14. W. Sun, S. Zhou, B. You, and L. Wu, *J. Mater. Chem. A*, 2013, **1**, 3146–3154.

15. Y. Jiang, P. Wan, M. Smet, Z. Wang, and X. Zhang, *Adv. Mater.*, 2008, **20**, 1972–1977.

16. W. Sun, S. Zhou, B. You, and L. Wu, *Macromolecules*, 2013, **46**, 7018–7026.

17. W. Sun, S. Zhou, B. You, and L. Wu, *J. Mater. Chem. A*, 2013, **1**, 10646.

18. M. Chen and F. Besenbacher, *ACS Nano*, 2011, **5**, 1549–1555.

Journal of Materials Chemistry A Accepted Manuscript

19. S. Patra, S. Sarkar, S. K. Bera, G. K. Paul, and R. Ghosh, *J. Appl. Phys.*, 2010, **108**, 083507.

20. M. Miyauchi, N. Kieda, S. Hishita, T. Mitsuhashi, A. Nakajima, T. Watanabe, and K. Hashimoto, *Surf. Sci.*, 2002, **511**, 401–407.

21. R. Wang, K. Hashimoto, A. Fujishima, M. Chikuni, E. Kojima, A. Kitamura, M. Shimohigoshi, and T. Watanabe, *Nature*, 1997, **388**, 431–432.

22. X. Feng, J. Zhai, and L. Jiang, *Angew. Chemie*, 2005, **44**, 5115–5118.

23. H. S. Lim, D. Kwak, D. Y. Lee, S. G. Lee, and K. Cho, *J. Am. Chem. Soc.*, 2007, **129**, 4128–4129.

24. S. Wang, Y. Song, and L. Jiang, *J. Photochem. Photobiol. C Photochem. Rev.*, 2007, **8**, 18–29.

25. N. Delorme, J.-F. Bardeau, A. Bulou, and F. Poncin-Epaillard, *Langmuir*, 2005, **21**, 12278–12282.

26. A. Athanassiou, M. I. Lygeraki, D. Pisignano, K. Lakiotaki, M. Varda, E. Mele, C. Fotakis, R. Cingolani, and S. H. Anastasiadis, *Langmuir*, 2006, **22**, 2329–2333.

27. L. Li, S. Pan, X. Pang, H. Chen, D. Hu, L. Ke, Y. Xiong, and W. Xu, *Soft Matter*, 2012, **8**, 7357–7360.

28. S. Abrakhi, S. Péralta, S. Cantin, O. Fichet, and D. Teyssié, *Colloid Polym. Sci.*, 2011, **290**, 423–434.

29. X. Pei, A. Fernandes, B. Mathy, X. Laloyaux, B. Nysten, O. Riant, and A. M. Jonas, *Langmuir*, 2011, **27**, 9403–9412.

30. M. Han, D. Ishikawa, T. Honda, E. Ito, and M. Hara, *Chem. Commun.*, 2010, **46**, 3598–600.

31. S. Abrakhi, S. Péralta, O. Fichet, D. Teyssié, and S. Cantin, *Langmuir*, 2013, **29**, 9499–9509.

32. D. Yang, M. Piech, N. S. Bell, D. Gust, S. Vail, A. a Garcia, J. Schneider, C.-D. Park, M. a Hayes, and S. T. Picraux, *Langmuir*, 2007, **23**, 10864–10872.

33. H. S. Lim, J. T. Han, D. Kwak, M. Jin, and K. Cho, *J. Am. Chem. Soc.*, 2006, **128**, 14458–14459.

34. C. Jin, R. Yan, and J. Huang, *J. Mater. Chem.*, 2011, **21**, 17519–17525.

35. F. Su, K. Chakrabarty, and R. B. Fair, *IEEE*, 2006, **25**, 211–223.

36. H. Akiyama, S. Kanazawa, Y. Okuyama, M. Yoshida, H. Kihara, H. Nagai, Y. Norikane, and R. Azumi, *ACS Appl. Mater. Interfaces*, 2014, **6**, 7933–41.

Journal of Materials Chemistry A Accepted Manuscript

37. V. R. Shembekar, a. Q. Contractor, S. S. Major, and S. S. Talwar, *Thin Solid Films*, 2006, **510**, 297–304.

38. R. Aich, F. Tran-Van, F. Goubard, L. Beouch, A. Michaleviciute, J. V. Grazulevicius, B. Ratier, and C. Chevrot, *Thin Solid Films*, 2008, **516**, 7260–7265.

39. W. Kohn and L. J. Sham, *Phys. Rev.*, 1965, **140**, A1133–A1138.

40. C. Lee, W. Yang, and R. G. Parr, *Phys. Rev. B*, 1988, **37**, 785–789.

41. A. D. Becke, *J. Chem. Phys.*, 1993, **98**, 5648–5652.

42. J.-D. Chai and M. Head-Gordon, *Phys. Chem. Chem. Phys.*, 2008, **10**, 6615–6620.

43. M. J. Frisch, G. W. Trucks, H. B. Schlegel, G. E. Scuseria, M. A. Robb, J. R. Cheeseman, G. Scalmani, V. Barone, B. Mennucci, G. A. Petersson, and others, *Gaussian, Inc., Wallingford, CT*, 2010.

44. E. Gross and W. Kohn, *Phys. Rev. Lett.*, 1985, **55**, 2850–2852.

45. E. Runge and E. K. U. Gross, *Phys. Rev. Lett.*, 1984, **52**, 997–1000.

46. E. K. U. Gross and W. Kohn, *Density Functional Theory of Many-Fermion Systems*, Elsevier, 1990, vol. 21.

47. R. Bauernschmitt and R. Ahlrichs, *Chem. Phys. Lett.*, 1996, **256**, 454–464.

48. M. E. Casida, C. Jamorski, K. C. Casida, and D. R. Salahub, *J. Chem. Phys.*, 1998, **108**, 4439–4449.

49. R. Dennington, T. Keith, and J. Millam, *Semichem Inc., Shawnee Mission KS*, 2009.

50. S. F. Boys and F. Bernardi, *Mol. Phys.*, 1970, **19**, 553–566.

51. Y. Zhang, P. Chen, and M. Liu, *Langmuir*, 2006, **22**, 10246–10250.

52. When the value is superior at 100%, the term of area ratio is no longer appropriate since there is probably an AzoC11 acid overlayer on TiO_2.

53. For the area ratio equal at 62%, the contact angle after irradiation should logically be between the contact angles of 39% and 77% of area ratios. However, this anomaly was reproducible on a large number of sample.

54. C. Radüge, G. Papastavrou, D. G. Kurth, and H. Motschmann, *Eur. Phys. journal. E*, 2003, **10**, 103–114.

55. N. Sarkar, S. Bhatta, and S. Sivaram, *Langmuir*, 1997, **13**, 4142–4149.

56. A. N. Shultz, W. Jang, W. M. Hetherington, D. R. Baer, L.-Q. Wang, and M. H. Engelhard, *Surf. Sci.*, 1995, **339**, 114–124.

Journal of Materials Chemistry A Accepted Manuscript

57. M. B. Hugenschmidt, L. Gamble, and C. T. Campbell, *Surf. Sci.*, 1994, **302**, 329–340.

58. A. Fahmi and C. Minot, *Surf. Sci.*, 1994, **304**, 343–359.

59. Mutsuyoshi Matsumoto, S. Terrettaz, and H. Tachibana, *Adv. colloid interface*, 2000, **87**, 147–164.

60. To induce *Cis→Trans* isomerization on our samples, we used a thermal way, blue light used in solution is not enough powerful.

61. M. Han, T. Honda, D. Ishikawa, E. Ito, M. Hara, and Y. Norikane, *J. Mater. Chem.*, 2011, **21**, 4696–4702.

62. D. Ishikawa, E. Ito, M. Han, and M. Hara, *Langmuir*, 2013, **29**, 4622–31.

63. F. V. Monteleone, G. Caputo, C. Canale, P. D. Cozzoli, R. Cingolani, D. Fragouli, and A. Athanassiou, *Langmuir*, 2010, **26**, 18557–63.

64. N. M. Ahmad, X. Lu, and C. J. Barrett, *J. Mater. Chem.*, 2010, **20**, 244–247.

65. Y.-N. Zhou, J.-J. Li, Q. Zhang, and Z.-H. Luo, *Langmuir*, 2014, **30**, 12236–12242.

66. N. Wagner and P. Theato, *Polymer*, 2014, **55**, 3436–3453.

67. R. Sun, A. Nakajima, A. Fujishima, T. Watanabe, and K. Hashimoto, *J. Phys. Chem. B.*, 2001, 1984–1990.

68. A. B. D. Cassie and S. Baxter, *Trans. Faraday Soc.*, 1944, **40**, 546–551.

69. Contact angles used in the Cassie-Baxter law for TiO_2 are from the reference 60.

Journal of Materials Chemistry A Accepted Manuscript

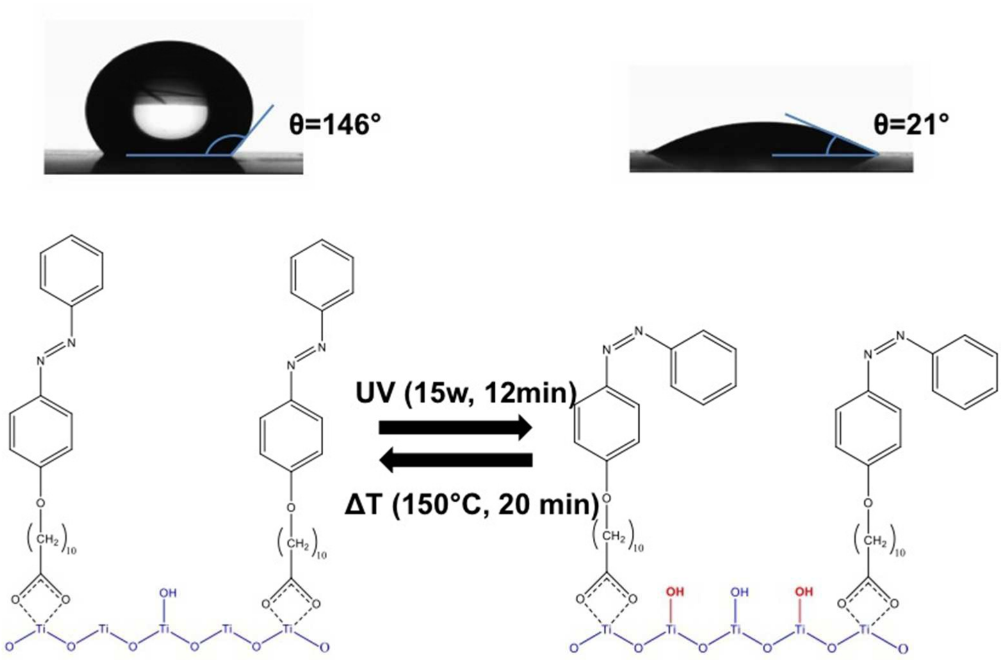

290x191mm (72 x 72 DPI)

Journal of Materials Chemistry A Accepted Manuscript